PHYSICAL REVIEW B **106**, L201401 (2022)

Letter   Editors' Suggestion

Single-exciton trapping in an electrostatically defined two-dimensional semiconductor quantum dot

Daniel N. Shanks,[1] Fateme Mahdikhanysarvejahany,[1] Michael R. Koehler,[2] David G. Mandrus,[3] Takashi Taniguchi,[4]
Kenji Watanabe,[5] Brian J. LeRoy,[1] and John R. Schaibley[1,*]
[1]*Department of Physics, University of Arizona, 1118 East 4th Street, Tucson, Arizona 85721, USA*
[2]*IAMM Diffraction Facility, Institute for Advanced Materials and Manufacturing, University of Tennessee, Knoxville,*
2641 Osprey Vista Way, Knoxville, Tennessee 37920, USA
[3]*Department of Materials Science and Engineering, University of Tennessee, Knoxville,*
1508 Middle Drive, Knoxville, Tennessee 37996, USA;
Materials Science and Technology Division, Oak Ridge National Laboratory, 1 Bethel Valley Road, Oak Ridge, Tennessee 37831, USA;
and Department of Physics and Astronomy, University of Tennessee, Knoxville, 1408 Circle Drive, Knoxville, Tennessee 37996, USA
[4]*International Center for Materials Nanoarchitectonics, National Institute for Materials Science, 1-1 Namiki, Tsukuba 305-0044, Japan*
[5]*Research Center for Functional Materials, National Institute for Materials Science, 1-1 Namiki, Tsukuba 305-0044, Japan*

(Received 27 June 2022; revised 9 October 2022; accepted 11 October 2022; published 3 November 2022)

Interlayer excitons (IXs) in two-dimensional semiconductors have long lifetimes and spin-valley coupled physics, with a long-standing goal of single-exciton trapping for valleytronic applications. In this work, we use a nanopatterned graphene gate to create an electrostatic IX trap. We measure a unique power-dependent blueshift of IX energy, where narrow linewidth emission exhibits discrete energy jumps. We attribute these jumps to quantized increases of the number occupancy of IXs within the trap and compare to a theoretical model to assign the lowest energy emission line to single-IX recombination.

DOI: 10.1103/PhysRevB.106.L201401

I. INTRODUCTION

WSe_2-$MoSe_2$ heterostructures are known to host spatially indirect excitons, with long (>1 ns) lifetimes due to the spatial separation of the electron and hole in different transition metal dichalcogenide (TMD) layers [1–7]. Signatures of multiple interlayer excitons (IXs) occupying a single trap have been observed in naturally occurring IX traps [8], and nanopillar-based strain induced traps [9]. In previous work, we demonstrated nanoscale trapping of IXs using nanopatterned graphene to induce a spatially varying electric field, which interacts with the permanent out of plane dipole moment of IXs to create an electrostatically defined quantum dot (QD) for IXs but were unable to resolve single-IX trapping [10]. In this work, we report discrete energy emission lines with a unique power dependence coming from an electrostatic IX QD, a signature of few-IX interactions and single-IX trapping. These traps are advantageous over other trapping methods involving strain or moiré traps, due to their deterministic placement in a lithographically defined process and 100 meV energy tunability by applied gate voltage, with potential for applications as optically active QD systems to serve as single-photon emitters or quantum spin–photon interfaces [11,12].

II. SAMPLE AND METHODS

Figures 1(a) and 1(b) show the layout of the electrostatic IX QD device, with an optical image of the device shown in the Supplemental Material [13] (Fig. S1). We used mechanical exfoliation and dry transfer to fabricate an hBN encapsulated WSe_2-hBN-$MoSe_2$ heterostructure, with top and bottom few layer graphene (FLG) gates. The thin hBN separator layer between the TMDs strongly reduces the induced moiré potential energy landscape and increases the dipole moment of the IXs, allowing for larger energy tunability of the IXs [14–16]. The TMD layers were angle aligned, with their crystal axes determined by second harmonic generation measurements [17–19]. The TMDs in this device have a near-zero degree twist angle (*R* type), determined by the energy and circular polarization of photoluminescence (PL) measurements on an adjacent region of the sample without the hBN spacer [16]. The top layer of hBN is chosen to be thin to allow for close proximity to the patterned top graphene layer. After the transfer step, we performed high resolution (100 kV) electron-beam lithography and O_2 reactive ion etch to pattern the graphene top gate, producing an oblong oval hole, measured to be 30×70 nm by atomic force microscopy (AFM), shown in Fig. 1(c). Previous studies have shown that hBN encapsulation of TMD layers preserves their optical properties under *e*-beam lithography exposure and O_2 etching, and that hBN is resistant to O_2 etching, which prevents the creation of processing-produced defects or trapping [20–22]. A second round of electron-beam lithography and thermal evaporation of Cr/Au was performed to electrically contact the sample.

Figure 1(d) shows the available energy states for inter- and intralayer excitons in a strong, spatially varying applied electric field underneath the etched graphene. The electric field profile created by the nanopatterned graphene was simulated in a three-dimensional (3D) COMSOL model, matching

---

[*] johnschaibley@arizona.edu

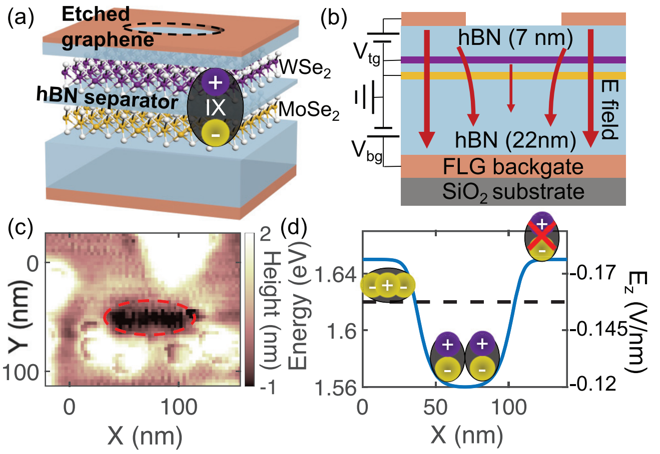

FIG. 1. Layout of the IX trapping structure. (a) Depiction of the MoSe$_2$-WSe$_2$ heterostructure, with a thin hBN spacer layer, encapsulated in hBN with a patterned graphene top gate and FLG back gate. (b) Depiction of the spatially varying electric field through the heterostructure. (c) AFM topography of the etched graphene hole, with the etched area outlined by the dashed red line. (d) Diagram of the inter- and intralayer exciton energy when the electric field is set such that the field away from the hole is -0.18 V/nm. The IX energy shifts with electric field due to the permanent out of plane dipole moment, while the intralayer exciton energy is unchanged.

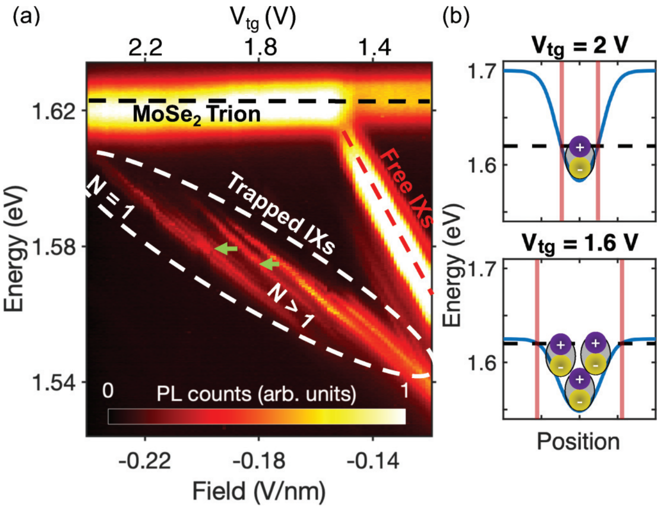

FIG. 2. (a) PL from a single-IX QD as a function of electric field, with excitation power 125 nW. The trapped IX PL shows discrete narrow emission lines, and energy shifts with electric field are shown by green arrows. The electric field axis refers to electric field strength away from the etched graphene. (b) Exciton energy near the etched graphene for varying applied voltage. Blue line indicates IX energy; black dashed line indicates MoSe$_2$ trion energy. Red lines mark the intersection, showing that with increasing applied voltage, there is less area where excitons will fall to the trapped IX state.

the shape of the graphene etch in the model to the AFM topography. The COMSOL simulations used an electrostatic model using known values for the in-plane and out of plane dielectric constants of the hBN, and hBN top layer thickness, that matched the AFM data of the individual 2D layers [23]. Voltage was applied at the top graphene-hBN interface, while the top surface of the TMD heterostructure was grounded. The minimum and maximum IX energies and field strengths are set to match the experimental data in Fig. 2.

III. EXPERIMENTAL RESULTS

With no applied electric field, the IX energy both underneath and away from the etched graphene is measured to be 1.4 eV, consistent with measurements on other hBN-separated MoSe$_2$-WSe$_2$ heterostructures [14–16]. When the electric field is applied in the opposite direction of the IX dipole moment, the IX energy increases proportionally to the strength of the local electric field by $\mathrm{H} = -\mathbf{p}\cdot\mathbf{E}$, where H is the IX energy, $\mathbf{p}$ is the permanent dipole moment of the IX, and $\mathbf{E}$ is the spatially varying electric field coming from the etched graphene. We calculate the electric field applied by the gate voltages using the three-plate capacitor model for the hBN-separated TMD layers, described in Unuchek *et al.* [14]. For a strong enough applied electric field, the IX energy can be tuned above the energy of the lowest available intralayer (MoSe$_2$) charged exciton state. However, because the electric field underneath the etched graphene is weaker, for a certain range of gate voltages, the lowest available energy state in this small area remains the trapped IX state.

Photoluminescence (PL) measurements were performed at 6 K in an optical cryostat (Montana Instruments), using a 670 nm diode laser and a grating-based spectrometer with a cooled CCD camera. We used a 0.6 NA 40× objective and a confocal pinhole which resulted in a collection diameter of 1.5 μm on the sample, aligned to the nanopatterned graphene oblong hole. Figure 2(a) shows gate-dependent photoluminescence (PL), where we applied a top gate–back gate voltage ratio equal to the relative thickness of the top and bottom hBN, $\alpha = -V_{bg}/V_{tg} = 3.2$, to apply an electric field while keeping the heterostructure overall charge neutral [24]. As the strength of the electric field increases, the PL energy from free IXs in the area surrounding the removed graphene and trapped IXs underneath the removed graphene increases linearly as expected.

At low electric field (less than -0.15 V/nm), the free IX PL signal shifts at a rate of 1.4 eV/(V/nm), leading to a measured dipole moment of 1.4 nm. At an electric field near -0.155 V/nm, the free IX energy is tuned to 1.62 eV, equal to the MoSe$_2$ intralayer trion energy. We note that the prevalence of the MoSe$_2$ trion at 1.62 eV and relatively weak signal from the MoSe$_2$ neutral exciton at 1.65 eV are consistent with the overall bilayer heterostructure being charge neutral, while the individual MoSe$_2$ and WSe$_2$ layers are doped equally and oppositely. At electric fields more negative than -0.16 V/nm, the IX energy would be higher than the MoSe$_2$ intralayer trion energy, but there is no observed PL signal from free IXs in this electric field regime. Additionally, the brightness from intralayer trions increases above this field, indicating that the population of holes in the MoSe$_2$ layer that would undergo charge transfer into the WSe$_2$ to create IXs no longer do so, resulting in a higher population of MoSe$_2$ intralayer particles. The trapped IX PL signal appears between 1.5 and 1.62 eV, and shows multiple, discrete narrow lines, with linewidths down to 0.9 meV. These lines can be attributed to electrostatically trapped IXs, as the reduced dipole shift is a signature of the weaker electric field experienced by these excitons underneath the removed graphene [10].

With increasing excitation power, the trapped IX signal is observed at higher energy (see Fig. S2 [13]). The higher laser power creates a higher density of excitons in the vicinity of the trap, resulting in higher trapped IX population. The observed PL energy shift can be attributed to IX-IX repulsion between IXs in the same trap, which comes from two different sources. One source is Coulomb dipolar repulsion energy $E_{p-p}(\Delta r)$ due to the repulsion of two dipoles at a distance Δr with their orientation locked to be parallel, previously observed in both semiconductor quantum well systems and TMD heterostructures [8,9,25–27]. The other source is IXs pushing themselves away from one another, up the sidewalls of the trap to an area of higher electrical potential energy $V_{\mathrm{IX}}(x, y)$ which depends on each IX position coordinates within the trap (x, y).

As the strength of the electric field increases, the trapped IX signal exhibits discrete shifts to lower energy states, indicating lower population of the trap. As the magnitude of the applied voltage is increased, there is less area on the sample where the IX state is lower energy than the MoSe$_2$ intralayer trion energy. Thus, there is less area where excitons fall to the IX state, producing a lower average occupation of the IX trap, shown by Fig. 2(b). At the strongest applied field (<-0.22 V/nm), when the lowest spatial IX energy in the center of the trap meets the MoSe$_2$ trion energy, the lowest PL emission line represents emission from a single trapped IX, as the system crosses the limiting case towards zero population of trapped IXs. We observe qualitatively similar discrete energy shifts in two other electrostatic QD structures (see Fig. S3 [13], and Refs. [28–30] therein).

We note a 10% increase in the slope of the dipole energy shift of the high population states ($–0.16\,\mathrm{V/nm} < E_z < –0.12\,\mathrm{V/nm}$) compared to the low population states ($E_z < –0.18\,\mathrm{V/nm}$) in Fig. 2(a). This change in dipole energy shift comes from IXs in high population states being pushed up the sidewalls of the trap, where the fractional electric field strength is larger. This confirms the electrostatic nature of the IX trap and rules out strain as the primary method of trapping, which would not produce a dipole shift which changes with population of the trap (see Figs. S4 and S5 [13]).

In order to characterize the discrete energy transitions, excitation power dependent PL was performed for low powers on the trapped IX signal, shown in Fig. 3(a). At the lowest measured excitation power, 8 nW, the lowest energy peak is most prominent and centered at 1561.44 ± 0.03 meV, with a small signal from a secondary peak at 1563.16 ± 0.05 meV. As the power is increased, the number of IXs in the QD increases. At 18 nW excitation power, the lowest energy PL peak becomes dimmer, and the second peak becomes the strongest, with a rise of a third peak at 1564.2± 0.1 meV. We attribute these three transitions to the lowest possible numbers of IX occupancy in the trap, $N = 1 \rightarrow 0$, $2 \rightarrow 1$, and $3 \rightarrow 2$ transitions of the IX population. Discrete power-dependent energy transitions such as these have been previously observed in MoSe$_2$-WSe$_2$ heterostructures [8,9], III-V quantum dots [31,32], and electrostatically trapped excitons in III-V coupled quantum wells [33], and are attributed to quantized numbers of IXs within these nanoscale traps. While single-photon emission is expected from a singly trapped exciton, a photon antibunching experiment was not performed here due to weak emission intensity from the sample.

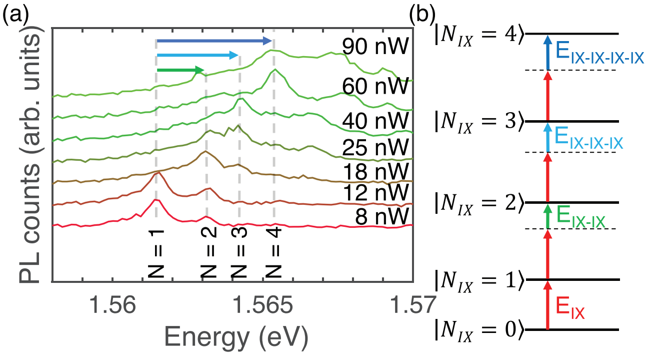

FIG. 3. Power-dependent PL on an IX QD. (a) PL for various laser excitation powers between 8 and 90 nW, with the gate voltage $V_{\mathrm{tg}} = –(1/\alpha)V_{\mathrm{bg}} = 1.8$ V, corresponding to an electric field strength away from the hole of -0.18 V/nm. Gray dashed lines indicated discrete emission peaks; green and blue arrows represent measured IX-IX repulsion energies. (b) Energy diagram of multiexciton states confined within the same QD. E_{IX} represents the lowest available energy state for a single IX at the applied electric field in the QD. $E_{\mathrm{IX}} + E_{\mathrm{IX-IX}}$ represents the additional energy to add a second IX to the same QD. $E_{\mathrm{IX}} + E_{\mathrm{IX-IX-IX}}$ ($E_{\mathrm{IX}} + E_{\mathrm{IX-IX-IX-IX}}$) represents the additional energy to add a third (fourth) IX to the QD.

Figure 3(b) shows the energy diagram and measured IX-IX repulsion energies for these transitions. We measure these experimental values by fitting the PL data to a multiple peak fit and taking the average of the center of these fits, with the uncertainty as the standard deviation of the center wavelength between different excitation power scans, with some representative fits shown in Fig. S6 [13]. Increasing the excitation power further causes the third peak to become the most prominent, with the eventual prominence of a fourth peak, until the linewidth broadens such that individual lines are no longer resolvable, representing a continuum of exciton states for excitation power above 5 μW, shown in Fig. S7 [13].

We consider other possible origins of the discrete jumps in the trapped IX PL signal, including charging of the QD with single electrons, and quantum confinement giving rise to quantized energy states. We rule out charging of the QD by the unique power-dependent blueshift of the IX peak in Fig. 3(a). In order to rule out the possibility of quantum confinement effects we estimated the quantum energy level spacing (see Supplemental Note I [13], and Ref. [34] therein), and found a lowest energy transition of 0.45 meV, four times lower than the lowest experimentally observed transition. Additionally, the quantum confinement would not produce the unique power dependence observed, where the lowest energy peak disappears with increasing power, and thus can be ruled as the source of these energy transitions.

IV. THEORETICAL MODEL

In these low power PL measurements, the dipole-dipole repulsion energy between IXs is on the order of 1–4 meV, consistent with the energy scale of multi-IX signatures in other reports [8,9]. We note that these previous results only report multiexciton states up to $N = 3$ [8] and $N = 5$ [9], whereas our electrostatic trap produces a significantly higher upper limit of multiexciton states, eventually producing a continuumlike state. In order to verify that the observed power-induced blueshift is indeed due to the lowest population IX transitions, we compare our data to a theoretical model for IXs. We calculated the expected IX repulsion energy by simulating the minimum energy positions of the IXs within the spatially varying potential, balancing dipole-dipole repulsion that pushes the IXs away from one another and the potential energy gradient induced by the etched graphene that pushes them together. This potential energy landscape for IXs is proportional to the electric field, which is determined by the COMSOL model of the structure. The dipole-dipole repulsion $E_{p-p}(\Delta r)$ is modeled using the bilayer Keldysh potential [35] as

$$E_{p-p}(\Delta r) = 2[V_k(\Delta r) - V_k(\sqrt{\Delta r^2 + d^2})], \qquad (1)$$

where Δr is the in-plane distance between the IXs and d is the measured vertical electron-hole separation of the excitons, 1.4 nm. The first term in parentheses in Eq. (1) represents the repulsive electron-electron and hole-hole potential energy between charges in the same layer, and the second term represents the attractive potential energy between electrons and holes in different IXs. $V_k(x)$ is the bilayer Rytova-Keldysh potential [35,36] which has been shown to model the electric potential created by charges in TMDs taking into account dielectric screening of the environment [37] (see Supplemental Note II [13], and Ref. [38] therein).

We minimize the total energy of the N-exciton system,

$$E_{N-\mathrm{IX}} = \frac{1}{2}\sum_{i,j} E_{p-p}(\Delta r_{ij}) + \sum_i V_{\mathrm{IX}}(x_i, y_i), \qquad (2)$$

where E_{p-p} is the dipolar repulsion term summed over all (i, j) exciton pairs with a $\frac{1}{2}$ term to account for double counting, and V_{IX} is the discretized spatial IX energy dependence of each individual IX given by the COMSOL electric field model. The minimum $V_{\mathrm{IX}} = 1.56\,\mathrm{eV}$ was set to match Fig. 3(a), and the maximum $V_{\mathrm{IX}} = 1.65\,\mathrm{eV}$ away from the etched graphene was determined by extrapolating the energy of free IXs to their value at the electric field $= -0.18\,\mathrm{V/nm}$, given the dipole shift of the free IX energy in Fig. 2(a). We use a numerical solver to minimize the IX energy, which was stable and reproducible for multiple IX initial locations within the trap. The quantum exchange integral term, which is repulsive for IXs in the same valley and zero for IXs in opposite valleys, was neglected in this simulation, as we are comparing our model to the lowest experimentally observed energy splitting, and the exchange energy term will only increase this energy splitting. Figure 4 shows the locations of IXs in some of the multi-IX simulations, and Table I shows the calculated multi-IX energies from the simulation in Fig. 4, compared to the experimental values in Fig. 3. $E_{\mathrm{IX-IX}} = E_{2-\mathrm{IX}} - 2(E_{\mathrm{IX}})$, where E_{IX} is the ground state energy of a single IX in the simulation, 1.56 eV, and $E_{2-\mathrm{IX}}$ is the minimum energy for two excitons in the trap as given by Eq. (2). $E_{\mathrm{IX-IX-IX}} = E_{3-\mathrm{IX}} - E_{2-\mathrm{IX}} - E_{\mathrm{IX}}$ is the additional potential energy from the third exciton in the trap, and $E_{\mathrm{IX-IX-IX-IX}} = E_{4-\mathrm{IX}} - E_{3-\mathrm{IX}} - E_{\mathrm{IX}}$.

TABLE I. Experimental multi-IX energies from Fig. 3 compared to simulated multi-IX energies from Fig. 4. All units are meV.

	$E_{\mathrm{IX-IX}}$	$E_{\mathrm{IX-IX-IX}}$	$E_{\mathrm{IX-IX-IX-IX}}$
Experiment	1.73 ± 0.05	2.8 ± 0.1	3.9 ± 0.1
Circular etch	3.9	5.6	7.9
Oblong etch	1.3	2.5	3.7
Oval etch	0.7	1.5	2.5

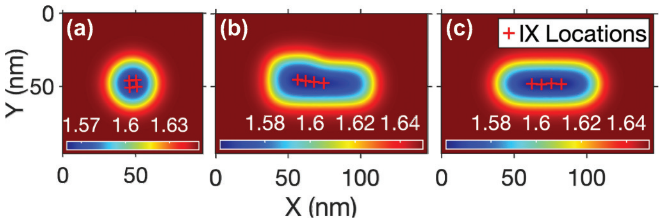

FIG. 4. Simulated locations for the four-exciton state for a circular trap of diameter 35 nm (a), an oblong shaped hole whose dimensions most closely match that of the AFM topography (b), and an oval hole of 30×70 nm (c). Color bar shows $V_{\mathrm{IX}}(x, y)$, whose spatial profile is determined from the COMSOL simulation of the electric field underneath the etched graphene. The minimum and maximum V_{IX} are set based on the measured data from Figs. 2 and 3.

The multi-IX energies from a circular graphene etch in Fig. 4(a) overestimate the measured multi-IX energy levels, while the oval hole in Fig. 4(c) slightly underestimates the observed multi-IX energies. We note that small changes in the etched graphene shape can produce significant changes in the IX repulsion energy. Upon careful investigation of the AFM topography, we observe that one side of the graphene etch is slightly wider than the other (see Fig. S8 [13]). Taking this into account, we modify our COMSOL simulation of the etched graphene shape to more closely represent the asymmetric shape determined by AFM topography, whose electric field profile is shown in Fig. 4(b). In this simulation, the multiexciton energies are within 25% of the experimentally measured values. Alternatively, this potential energy landscape would also accurately represent the oval graphene etch in Fig. 4(c), with a small change in the potential energy across the length of the hole due to randomly induced potential energy variation across the sample described in Mahdikhanysarvejahany *et al.* [16], possibly due to strain [39].

V. CONCLUSION

In conclusion, we observe evidence of single- and few-IX trapping in an electrostatically defined 2D semiconductor quantum dot. Our approach using patterned graphene gates is highly customizable and results in location-specific placement of the quantum dot as well as highly tunable emission energies via gate voltage. While there has been recent progress in alternative methods to lithographically define quantum dots in TMD systems that involve direct patterning of the semiconducting material [20,21,40], our approach leaves the TMD crystal intact, neutralizing the effect of edge states. Future studies will involve QD-trapped excitons in a magnetic field to break valley degeneracy, creating a valley-based two-level system, or investigating the ability to controllably charge the quantum dot with single electrons to realize a highly deterministic spin-photon interface [41], which can be potentially interfaced with nanoplasmonic waveguides to realize single-photon transistors [42] and quantum repeaters [11].

ACKNOWLEDGMENTS

The authors acknowledge useful conversations with Dr. Rolf Binder. J.R.S. and B.J.L. acknowledge support from the National Science Foundation Grants No. ECCS-2054572 and No. DMR-2003583, and the Army Research Office under Grant No. W911NF-20-1-0215. J.R.S. acknowledges support from Air Force Office Scientific Research Grants No. FA9550-18-1-0390 and No. FA9550-21-1-0219. B.J.L. acknowledges support from the Army Research Office under Grant No. W911NF-18-1-0420 and the National Science Foundation Grant No. ECCS- 2122462. D.G.M. acknowledges support from the Gordon and Betty Moore Foundation's EPiQS Initiative, Grant No. GBMF9069. K.W. and T.T. acknowledge support from JSPS KAKENHI (Grants No. 19H05790, No. 20H00354, and No. 21H05233). Plasma etching was performed using a Plasma-Therm reactive ion etcher acquired through an NSF MRI grant, Award No. ECCS-1725571.

[1] P. Rivera, J. R. Schaibley, A. M. Jones, J. S. Ross, S. Wu, G. Aivazian, P. Klement, K. Seyler, G. Clark, N. J. Ghimire *et al.*, Observation of long-lived interlayer excitons in monolayer $MoSe_2$-WSe_2 heterostructures, Nat. Commun. **6**, 6242 (2015).

[2] J. R. Schaibley, P. Rivera, H. Yu, K. L. Seyler, J. Yan, D. G. Mandrus, T. Taniguchi, K. Watanabe, W. Yao, and X. Xu, Directional interlayer spin-valley transfer in two-dimensional heterostructures, Nat. Commun. **7**, 13747 (2016).

[3] J. R. Schaibley, H. Yu, G. Clark, P. Rivera, J. S. Ross, K. L. Seyler, W. Yao, and X. Xu, Valleytronics in 2D materials, Nat. Rev. Mater. **1**, 11 (2016).

[4] J. S. Ross, P. Rivera, J. R. Schaibley, E. Lee-Wong, H. Yu, T. Taniguchi, K. Watanabe, J. Yan, D. G. Mandrus, D. Cobden *et al.*, Interlayer exciton optoelectronics in a 2D heterostructure *p-n* junction, Nano Lett. **17**, 638 (2017).

[5] P. Rivera, H. Yu, K. L. Seyler, N. P. Wilson, W. Yao, and X. Xu, Interlayer valley excitons in heterobilayers of transition metal dichalcogenides, Nat. Nanotechnol. **13**, 1004 (2018).

[6] P. Nagler, F. Mooshammer, J. Kunstmann, M. V. Ballottin, A. Mitioglu, A. Chernikov, A. Chaves, F. Stein, N. Paradiso, S. Meier *et al.*, Interlayer excitons in transition-metal dichalcogenide heterobilayers, Phys. Status Solidi B **256**, 1900308 (2019).

[7] F. Mahdikhanysarvejahany, D. N. Shanks, C. Muccianti, B. H. Badada, I. Idi, A. Alfrey, S. Raglow, M. R. Koehler, D. G. Mandrus, T. Taniguchi *et al.*, Temperature dependent moiré trapping of interlayer excitons in $MoSe_2$-WSe_2 heterostructures, npj 2D Mater. Appl. **5**, 67 (2021).

[8] W. Li, X. Lu, S. Dubey, L. Devenica, and A. Srivastava, Dipolar interactions between localized interlayer excitons in van der Waals heterostructures, Nat. Mater. **19**, 624 (2020).

[9] M. Kremser, M. Brotons-Gisbert, J. Knörzer, J. Gückelhorn, M. Meyer, M. Barbone, A. V. Stier, B. D. Gerardot, K. Müller, and J. J. Finley, Discrete interactions between a few interlayer excitons trapped at a $MoSe_2$-WSe_2 heterointerface, npj 2D Mater. Appl. **4**, 8 (2020).

[10] D. N. Shanks, F. Mahdikhanysarvejahany, C. Muccianti, A. Alfrey, M. R. Koehler, D. G. Mandrus, T. Taniguchi, K. Watanabe, H. Yu, B. J. LeRoy *et al.*, Nanoscale trapping of interlayer excitons in a 2D semiconductor heterostructure, Nano Lett. **21**, 5641 (2021).

[11] I. Aharonovich, D. Englund, and M. Toth, Solid-state single-photon emitters, Nat. Photon. **10**, 631 (2016).

[12] D. J. Morrow and X. Ma, Trapping interlayer excitons in van der Waals heterostructures by potential arrays, Phys. Rev. B **104**, 195302 (2021).

[13] See Supplemental Material at http://link.aps.org/supplemental/10.1103/PhysRevB.106.L201401 for details on the quantum confinement calculation, Keldysh potential, optical image of the device, extended power and electric field dependent PL data, PL data from alternate QD sites, calculated multi-IX energies as a function of electric field, representative fits to PL data, and extended AFM data of the etched graphene hole.

[14] D. Unuchek, A. Ciarrocchi, A. Avsar, Z. Sun, K. Watanabe, T. Taniguchi, and A. Kis, Valley-polarized exciton currents in a van der Waals heterostructure, Nat. Nanotechnol. **14**, 1104 (2019).

[15] D. N. Shanks, F. Mahdikhanysarvejahany, T. G. Stanfill, M. R. Koehler, D. G. Mandrus, T. Taniguchi, K. Watanabe, B. J. LeRoy, and J. R. Schaibley, Interlayer exciton diode and transistor, Nano Lett. **22**, 6599 (2022).

[16] F. Mahdikhanysarvejahany, D. N. Shanks, M. Klein, Q. Wang, M. R. Koehler, D. G. Mandrus, T. Taniguchi, K. Watanabe, O. L. A. Monti, B. J. LeRoy *et al.*, Localized interlayer excitons in $MoSe_2$-WSe_2 heterostructures without a moiré potential, Nat. Commun. **13**, 5354 (2022).

[17] N. Kumar, S. Najmaei, Q. Cui, F. Ceballos, P. M. Ajayan, J. Lou, and H. Zhao, Second harmonic microscopy of monolayer MoS_2, Phys. Rev. B **87**, 161403(R) (2013).

[18] L. M. Malard, T. V. Alencar, A. P. M. Barboza, K. F. Mak, and A. M. de Paula, Observation of intense second harmonic generation from MoS_2 atomic crystals, Phys. Rev. B **87**, 201401(R) (2013).

[19] H. Zeng, G. B. Lui, J. Dai, Y. Yan, B. Zhu, R. He, L. Xie, S. Xu, X. Chen, W. Yao *et al.*, Optical signature of symmetry variations and spin-valley coupling in atomically thin tungsten dichalcogenides, Sci. Rep. **3**, 1608 (2013).

[20] T. K. Stanev, P. Liu, H. Zeng, E. J. Lenferink, A. A. Murthy, N. Speiser, K. Watanabe, T. Taniguchi, V. P. Dravid, and N. P. Stern, Direct patterning of optoelectronic nanostructures using encapsulated layered transition metal dichalcogenides, ACS Appl. Mater. Interf. **14**, 23775 (2022).

[21] D. Yagodkin, K. Greben, A. E. Ascunce, S. Kovalchuk, M. Ghorbani-Asl, M. Jain, S. Kretschmen, N. Severin, J. Rabe, A. V. Krasheninnikov *et al.*, Extrinsic localized excitons in patterned 2D semiconductors, Adv. Funct. Mater. **32**, 2203060 (2022).

[22] Z. Liu, Y. Gong, W. Zhou, L. Ma, J. Yu, J. C. Idrobo, J. Jung, A. H. MacDonald, R. Vajtai, J. Lou *et al.*, Ultrathin high-temperature oxidation-resistant coatings of hexagonal boron nitride, Nat. Commun. **4**, 2541 (2013).

[23] A. Laturia, M. L. Van de Put, and W. G. Vandenberghe, Dielectric properties of hexagonal boron nitride and transition metal dichalcogenides: From monolayer to bulk, npj 2D Mater. Appl. **2**, 6 (2018).

[24] L. A. Jauregui, A. Y. Joe, K. Pistunova, D. S. Wild, A. A. High, Y. Zhou, G. Scuri, K. De Greve, A. Sushko, C. H. Yu *et al.*, Electrical control of interlayer exciton dynamics in atomically thin heterostructures, Science **366**, 870 (2019).

[25] L. V. Butov, A. A. Shashkin, V. T. Dolgopolov, K. L. Campman, and A. C. Gossard, Magneto-optics of the spatially separated electron and hole layers in GaAs/$\mathrm{Al}_x\mathrm{Ga}_{1-x}$As coupled quantum wells, Phys. Rev. B **60**, 8753 (1999).

[26] B. Laikhtman and R. Rapaport, Exciton correlations in coupled quantum wells and their luminescence blue shift, Phys. Rev. B **80**, 195313 (2009).

[27] Z. Sun, A. Ciarrocchi, F. Tagarelli, J. F. Gonzalez Marin, K. Watanabe, T. Taniguchi, and A. Kis, Excitonic transport driven by repulsive dipolar interaction in a van der Waals heterostructure, Nat. Photon. **16**, 79 (2022).

[28] R. Rosati, S. Brem, R. Perea-Causín, R. Schmidt, I. Niehues, S. M. de Vasconcellos, R. Bratschitsch, and E. Malic, Strain-dependent exciton diffusion in transition metal dichalcogenides, 2D Mater. **8**, 015030 (2020).

[29] M. G. Harats, J. N. Kirchhof, M. Qiao, K. Greben, and K. I. Bolotin, Dynamics and efficient conversion of excitons to trions in non-uniformly strained monolayer WS_2, Nat. Photon. **14**, 324 (2020).

[30] T. P. Darlington, C. Carmesin, M. Florian, E. Yanev, O. Ajayi, J. Ardelean, D. Rhodes, A. Ghiotto, A. Krayev, K. Watanabe *et al.*, Imaging strain-localized excitons in nanoscale bubbles of monolayer WSe_2 at room temperature, Nat. Nanotechnol. **15**, 854 (2020).

[31] A. Zrenner, A close look on single quantum dots, J. Chem. Phys. **112**, 7790 (2000).

[32] J. J. Finley, A. D. Ashmore, A. Lemaître, D. J. Mowbray, M. S. Skolnick, I. E. Itskevich, P. A. Maksym, M. Hopkinson, and T. F. Krauss, Charged and neutral exciton complexes in individual self-assembled In(Ga)As quantum dots, Phys. Rev. B **63**, 073307 (2001).

[33] G. J. Schinner, J. Repp, E. Schubert, A. K. Rai, D. Reuter, A. D. Wieck, A. O. Govorov, A. W. Holleitner, and J. P. Kotthaus, Confinement and Interaction of Single Indirect Excitons in a Voltage-Controlled Trap Formed Inside Double InGaAs Quantum Wells, Phys. Rev. Lett. **110**, 127403 (2013).

[34] H. Yu, Y. Wang, Q. Tong, X. Xu, and W. Yao, Anomalous Light Cones and Valley Optical Selection Rules of Interlayer Excitons in Twisted Heterobilayers, Phys. Rev. Lett. **115**, 187002 (2015).

[35] H. C. Kamban and T. G. Pedersen, Interlayer excitons in van der waals heterostructures: Binding energy, Stark shift, and field-induced dissociation, Sci. Rep. **10**, 5537 (2020).

[36] L. V. Keldysh, Coulomb interaction in thin semiconductor and semimetal films, Sov. Phys. JETP Lett. **29**, 658 (1979).

[37] A. Chernikov, T. C. Berkelbach, H. M. Hill, A. Rigosi, Y. Li, B. Aslan, D. R. Reichman, M. S. Hybertsen, and T. F. Heinz, Exciton Binding Energy and Nonhydrogenic Rydberg Series in Monolayer WS_2, Phys. Rev. Lett. **113**, 076802 (2014).

[38] T. C. Berkelbach, M. S. Hybertsen, and D. R. Reichman, Theory of neutral and charged excitons in monolayer transition metal dichalcogenides, Phys. Rev. B **88**, 045318 (2013).

[39] W. Wang and X. Ma, Strain-induced trapping of indirect excitons in MoSe_2/wse_2 heterostructures, ACS Photon. **7**, 2460 (2020).

[40] G. Wei, D. A. Czaplewski, E. J. Lenferink, T. K. Stanev, I. W. Jung, and N. P. Stern, Size-tunable lateral confinement in monolayer semiconductors, Sci. Rep. **7**, 3324 (2017).

[41] M. Atatüre, D. Englund, N. Vamivakas, S.-Y. Lee, and J. Wrachtrup, Material platforms for spin-based photonic quantum technologies, Nat. Rev. Mater. **3**, 38 (2018).

[42] D. E. Chang, A. S. Sørensen, E. A. Demler, and M. D. Lukin, A single-photon transistor using nanoscale surface plasmons, Nat. Phys. **3**, 807 (2007).